Int. J. Electrochem. Sci., 10 **(2015)** 3510 - 3517

International Journal of
ELECTROCHEMICAL
SCIENCE
www.electrochemsci.org

Short Communication

Interlayer Distance Dependency of Lithium Storage in MoS_2 as Anode Material for Lithium-ion Batteries

Xiaofang Qian, Yourong Wang[*]*, Wei Zhou, Liping Zhang, Guangsen Song and Siqing Cheng*[*]

Innovation Center for Nanomaterials in Energy and Medicine (ICNEM), School of Chemical and Environmental Engineering, Wuhan Polytechnic University, Hubei 430023, P. R. China
[*]E-mail: icnem@hotmail.com

Received: 9 January 2015 / *Accepted:* 10 February 2015 / *Published:* 24 February 2015

Polyvinyl pyrrolidone (PVP) as dispersant was employed to assist the hydrothermal synthesis of MoS_2. The results show that the interlayer distance of the as-obtained MoS_2 is smaller compared with the original MoS_2 without PVP-assistance using XRD, SEM and TEM techniques for characterization. Investigations of the electrochemical performances of MoS_2 with different interlayer distance as anode material for LIBs demonstrate that the specific capacity and the cycling performance of lithium storage of MoS_2 is significantly dependent on the interlayer distance of MoS_2, furthermore causing the different mechanism of lithium storage. This might be attributed to the varied internal resistance and Li-ion diffusion in layered MoS_2 due to the different interlayer distance, which is validated from electrochemical impedance spectroscope of MoS_2 electrode.

Keywords: MoS_2; Anode material; Interlayer distance; Lithium-ion battery.

1. INTRODUCTION

Considerable efforts have been devoted to rechargeable Li-ion batteries (LIBs) due to the ever-increasing demands for energy conversion and storage worldwide, in particular, as power sources for high power tools and electric vehicles.[1-3] Graphite is extensively utilized as a commercial anode material in LIBs owing to its low and flat potential profile for lithium intercalation and structural stability during cycling. However, the low theoretical capacity of graphite (372 mAh g^{-1}), which restricts its use for next-generation battery applications in its current status, makes it critical to find

alternative anode materials paired with the lithiated cathode with high energy densities and high capacity.[4]

To circumvent these problems, some metal and metal oxides (such as Sn, Si, SnO_2, Co_3O_4 etc.) as alternative anode materials for graphite have attracted considerable interest due to their high specific capacity.[5-6] However, these materials can be easily suffering large volume changes and accompanying sharp decreases in capacity that occur during electrochemical cycles, thus their practical applications were largely restricted.[7-8] Recently, a new class of cost-effective, low-dimensional layered transition metal dichalcogenide compounds MX_2 (M =Mo, Ti, V, W; X=S, Se, Te) have been introduced in the literature due to their typical sandwich layered structure analogous to graphite and their unique properties.[9] Among them molybdenum disulfide (MoS_2) has received a tremendous amount of interest as a promising anode material at low voltage for LIBs with its high theoretical capacity of 670 mAh g^{-1} assuming 4 moles of Li^+ insertion to form the products Li_2S and Mo.[10-12] Compared to graphite, the interlayer distance between neighboring layers is 0.615 nm, significantly larger than that of graphite (0.335 nm), which is more suitable for Li-ion chemical intercalation and diffusion. Furthermore, in the layered MoS_2, atoms are first bound by strong ionic/covalent forces to form two-dimensional layers (nanosheets) that stacked by weak van der Waals interaction, which allows Li ions to diffuse without a significant increase in volume. As such, the interlayer distance of MoS_2 is vital to improve the electrochemical performance of MoS_2 as anode material for LIBs, which is significantly influenced by the morphology, structure, and particle size of the materials. So far, many research groups have devoted to enhancing the electrochemical performances of MoS_2-based anodes by enlarging the interlayer distance of MoS_2 via tuning the morphology, structure and particle size of MoS_2, such as MoS_2 nanoflowered structures by various techniques [13-14], overlayers supported on coaxial carbon nanotubes, CNT-MoS_2 hybrid materials by solvothermal synthesis[15-16], glucose assisted growth of nanosheets of MoS_2 on the CNT backbone by a hydrothermal method[17], α–MoO_3 as a precursor to prepare MoS_2 nanorods followed by their coating with amorphous carbon[18], MoS_2 nanotubes by hydrothermal intercalation and exfoliation route[19] etc. Consequently, the electrochemical performance of MoS_2 as anode for LIBs is significantly dependent on the interlayer distance between layers.

Herein, we employed PVP as dispersant to assist the hydrothermal synthesis of MoS_2 for tuning the interlayer distance of MoS_2 and investigated the electrochemical performance dependence of interlayer distance of MoS_2.

2. EXPERIMENTAL SECTION

2.1 Synthesis of MoS_2 samples

All chemicals used in this experiment were of analytical grade and used directly without further purification. In a typical batch, 3.7 g of ammonium heptamolybdate tetrahydrate (AHM: $(NH_4)_6Mo_7O_{24}\cdot 4H_2O$, 3 mmol) and 0.7 g of sulfocarbamide (SC: $CS(NH_2)_2$), 9 mmol) were dissolved

in 70 mL of deionized water. Then, 10 M HCl was added to the solution drop by drop until the pH value of the solution was 4. After 30 min of stirring, the solution was transferred to a 100 mL Teflon-lined stainless steel autoclave, sealed tightly and thermostated at 200 °C overnight. After cooling naturally, the product was separated by centrifugation and washed ultrasonically with deionized water and absolute ethanol for several times before drying in a vacuum oven at 60 °C for 24 h. The as-prepared MoS_2 was designated as MS. Keeping under the same experimental conditions, 0.1 g of polyvinyl pyrrolidone (PVP) was added to the initial solution to synthesis MoS_2, which was designated as PMS.

2.2 Materials characterization

The X-ray diffraction (XRD) patterns were obtained on a Shimadzu XRD-600 diffractometer operating with Cu Kα radiation (λ = 1.5418 Å) at a scanning step of 2º per minute. Transmission electron microscope (TEM) images were acquired with a transmission electron microscope of JEM-2010 at an accelerating voltage of 100 kV and the samples were prepared by dipping an amorphous carbon-copper grid in a dilute solution of samples dispersed in absolute ethanol. Scanning electron microscope (SEM) images were acquired from a Hitachi field emission scanning electron microscope and the samples were prepared by sonicating the products in absolute ethanol and evaporating one drop of suspension on conductive adhesive.

2.3 *Electrochemical measurements*

The working electrodes were prepared by 70 wt% active materials (MS or PMS), 20 wt% carbon black, and 10 wt% poly(vinylidene fluoride) (PVDF) dissolved in N-methylpyrrolidone (NMP) on a copper foil. Then, the coated copper foil was dried under vacuum at 80 °C for 24 h and cut into pieces with a diameter of 12 mm before use. A Celgard 2600 membrane was used as a separator between the working electrode and the counter electrode (Lithium metal foil). The electrolyte was 1 M $LiPF_6$ in a mixture of ethylene carbonate (EC)/diethyl carbonate (DEC) (1:1 by volume). Thus, the 2016 coin-type cells were assembled in an Ar-filled glove box. Galvanostatic charge/discharge cycles of the cells were conducted between 0.02 and 3.00 V on a LAND CT-2001A battery cycler (Wuhan, China) at room temperature. Cyclic voltammetry (CV) profiles (0.02 – 3.00 V, 0.2 mV s^{-1}) were obtained on an electrochemical workstation (CHI 660D, Shanghai, China). Electrochemical impedance spectroscopy (EIS) was obtained by applying a sine wave with amplitude of 5.0 mV over the frequency range from 100 kHz to 0.01 Hz.

3. RESULTS AND DISCUSSION

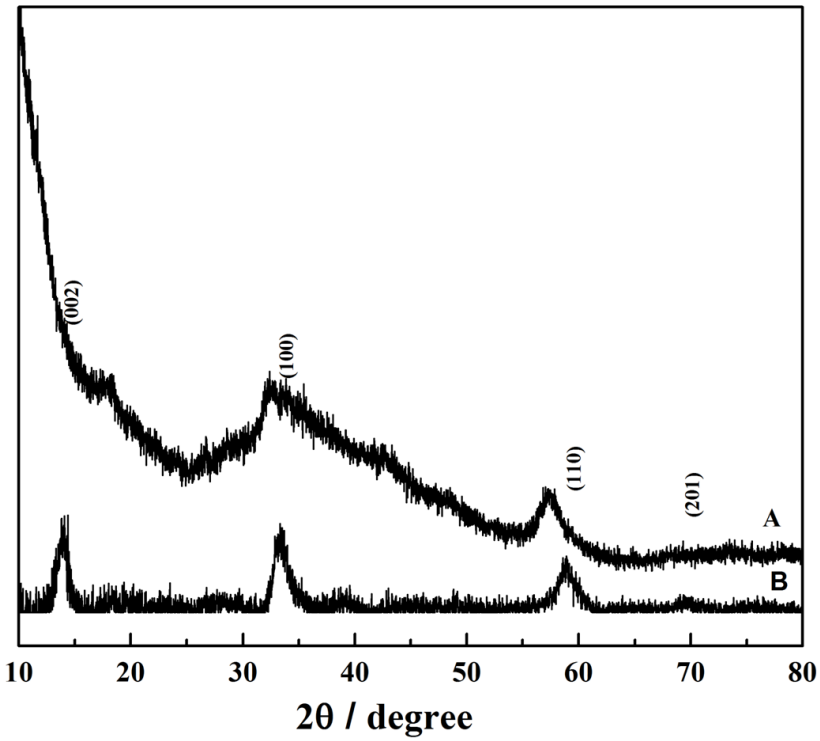

Figure 1. XRD patterns of the as-prepared MS (B) and PMS (A) nanoparticles

Figure 1 shows the XRD patterns of the as-obtained products, indicating the single phase of MS and PMS. All the diffraction peaks in the patterns can be indexed as hexagonal-phase MoS_2 (JCPDS No. 37-1492) which belongs to the space group $P6_3/mmc$ (No. 194). All peaks are not very sharp, indicating not pretty good crystallization because the as-obtained samples were not annealed before use, which does not influence the electrochemical performance of MS and PMS. The characteristic [002] peak signifies a stacked layered structure.[20] The obvious [002] peak in Fig.1B for MS nanoparticles reveals the restacking of MoS_2 layers. According to Bragg's equation, it can be calculated that the mean interlayer distance of the adjacent single-layer MoS_2 sheets in the composite is about 0.98 nm, which is much larger than that of standard MoS_2 (0.615 nm)[21]. However, in Fig. 1A for PMS nanoparticles, the [002] peak almost disappears, which should be attributed to two possible cases: (1) the restacking of MoS_2 layer sheets doesn't take place; (2) the MoS_2 layer sheets are restacked tightly almost without any space between layer sheets. For PMS, PVP used as dispersant might damage the van der Waals forces for the layer stacking of MoS_2 nanosheets to result in the aggregation of MoS_2 nanosheets. As such, the absence of the [002] peak might result from the second case, i.e. the interlayer distance between MoS_2 nanosheets almost approaches to zero, which is much smaller than that of standard MoS_2. Furthermore, the weak [002] peak in Fig. 1B shifts to larger diffraction angle compared to that in Fig. 1A, indicating the smaller interlayer distance for PMS and the aggregation of MoS_2 nanosheets. All these could be further illustrated visually by TEM and SEM

images of the as-obtained products, as shown in Fig. 2. It can be seen that MS displays nanoflowered structure consisting of MoS_2 nanosheets while PMS is a solid nanosphere (ca. 100 nm) with loose brim. Thus, MoS_2 with different interlayer distance is fabricated and the interlayer distance of MS is much larger than that of PMS.

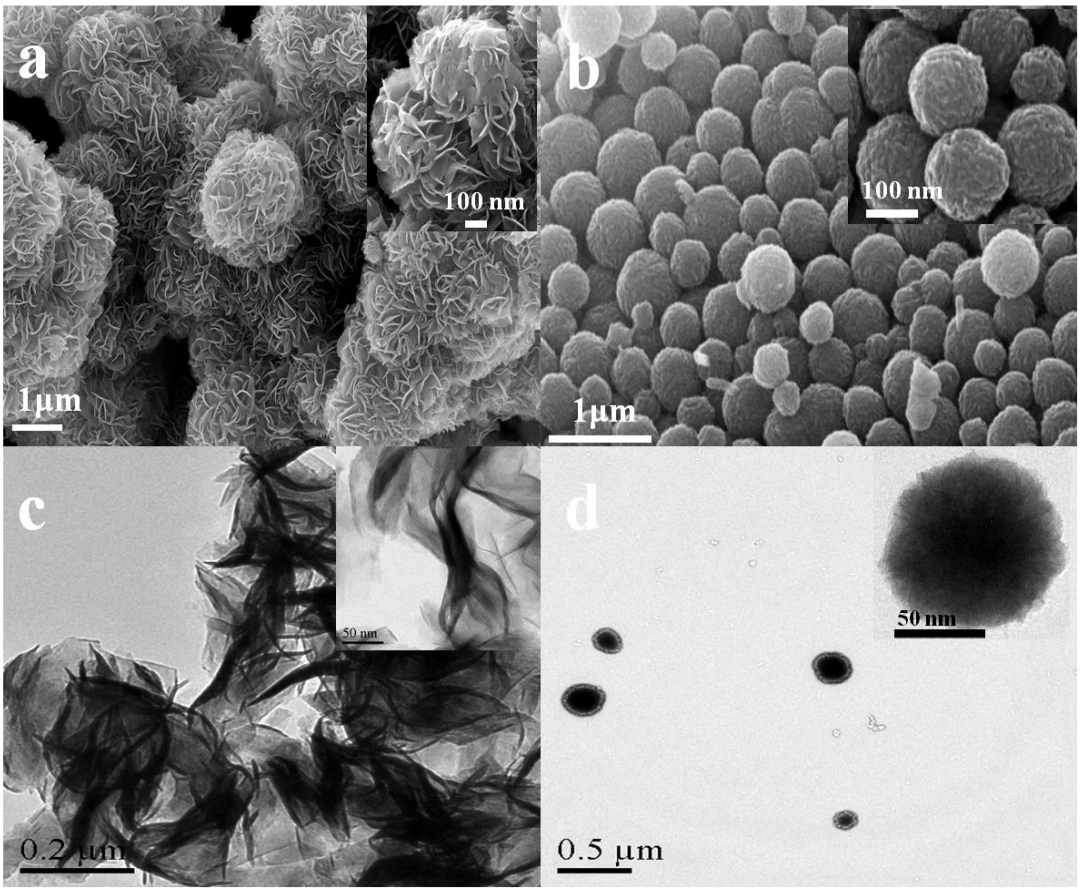

Figure 2. SEM and TEM images of MS (a,c) and PMS (b, d). The inserted images on the left of every image are the local enlarged regions.

Electrochemical properties of MS and PMS electrodes have been investigated by cyclic voltammetry (CV) and galvanostatic charge-discharge experiments. Fig. 3a shows the initial cyclic voltammograms of MS and PMS electrodes at a scan rate of 0.2 mV s^{-1} in the potential window of 0.02 – 3.00 V. For MS electrode, two reduction peaks (at ~1.0 V and ~ 0.5 V) and two oxidation peaks (at ~1.8 V and ~ 2.25 V) are observed. The reduction peak at ~1.0 V can be attributed to the structural change of MoS_2 from trigonal prismatic to octahedral coordination while lithium ions intercalate into MoS_2 as reported in literature[22], and the other reduction peak at ~ 0.5 V attributed to a conversion reaction process of MoS_2 into Mo nanoparticles embedded in a Li_2S matrix[23].

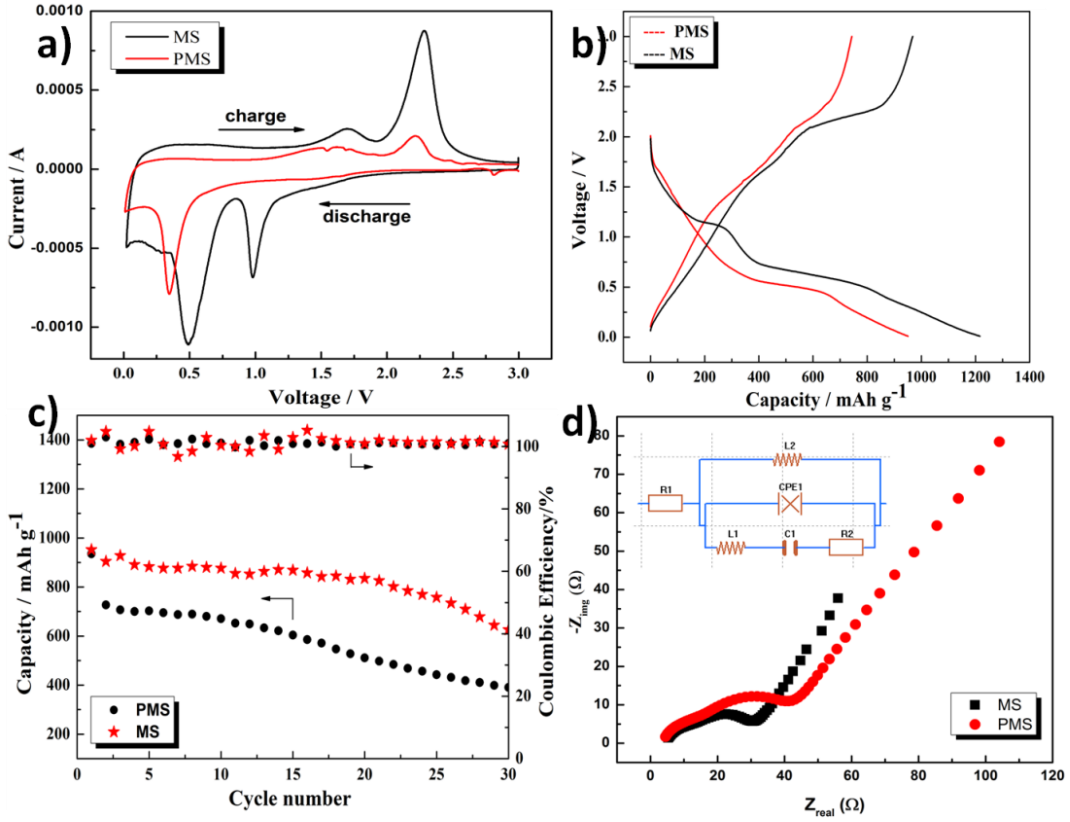

Figure 3. (a) Cyclic voltammograms of MS and PMS electrodes vs. Li at a scan rate of 0.2 mV s^{-1} during the first cycle, (b) initial galvanostatic charge-discharge profiles of MS and PMS electrodes at 100 mA g^{-1} in the voltage range of 0.02-3V *vs.* Li^+/Li, (c) cycling performance and coulombic efficiency of MS and PMS electrodes at 400 mA g^{-1}, and (d) Nyquist plots of MS and PMS electrodes obtained by applying a sine wave with an amplitude of 5.0 mV over the frequency range from 100 KHz to 0.01 Hz, the insert shows the equivalent circuit model of the studied system.

Meanwhile, the oxidation peak at ~1.8 V can be attributed to partial oxidation of Mo to form MoS_2 while the other oxidation peak at ~ 2.25 V is attributed to the formation of MoS_2.[12, 24] However, for PMS electrode, one obvious (at ~ 0.3 V) and one weak reduction peak (at ~ 2.7 V) are appeared in lithiation process. Obviously, the main reduction peak at ~ 0.3 V could be attributed to the conversion process where Li_xMoS_2 are transformed into Mo/Li_2S nanocomposite while the weak reduction peak at ~ 2.7 V should be explained by the formation of a gel-like polymeric layer.[22] The similar two oxidation peaks for PMS electrode compared to MS electrode reveals the similar dilithiation process. This reflects lithium storage dependence of interlayer distance of layered MoS_2. With increasing the interlayer distance, lithiation process might result in the structural change in MoS_2 followed by the conversion process of MoS_2 to Mo and Li_2S while in certain interlayer distance for lithiation process, the structure change doesn't occur but directly proceeds to the conversion process of MoS_2 to Mo nanoparticles and Li_2S. In contrast, delithiation process is not relative to the interlayer

distance. Moreover, the correlative plateau regions can be identified in the charge-discharge profiles of MS and PMS electrodes at 100 mA g^{-1} rate, as shown in Fig.3b. The first discharge curve for MS electrode shows two insertion plateaus at ~1.0 V and ~ 0.5 V while only one insertion plateau at ~ 0.3 V for PMS is observed, thus resulting in the significantly different discharge capacity. Obviously, MS electrode delivers an initial discharge capacity of 1216 mA h g^{-1} at 100 mA g^{-1} while PMS electrode only exhibits an initial discharge capacity of 950 mAh g^{-1}.

Fig. 3c shows the cycling performances and coulombic efficiencies of MS and PMS electrodes evaluated at 400 mA g^{-1} between 0.02 and 3.00 V *vs.* Li^+/Li. The initial discharge capacity for MS and PMS at 400 mA g^{-1} are 935 and 932 mAh g^{-1}, respectively, corresponding to coulombic efficiencies of 100%, showing reversible electrochemical performances of MS and PMS electrodes. For MS electrode, the reversible capacity still remains as high as 883 mAh g^{-1} at 400 mA g^{-1} after 30 cycles, with a capacity retention of 94.4%, indicating excellent cycling performance. On contrary, the reversible capacity of PMS electrode at 400 mA g^{-1} after 30 cycles decays to 391 mAh g^{-1}, showing the poor cycling performance. Consequently, the electrochemical performance is determined by the interlayer distance in MoS_2.

In order to further gain the insight into the rationale of the difference in electrochemical performances of MS and PMS electrodes, we carried out electrochemical impedance spectroscopy (EIS) analyses of MS and PMS electrodes. Fig. 3d shows typical Nyquist plots of MS and PMS electrodes and the equivalent circuit model of the studies systems. Generally, the Nyquist plosts are composed of a semicircle at high frequency and medium frequency and an inclined line in the low frequency region. The high-frequency intercept on the real axis represents the ohmic resistance of the cell, including the electrolyte and electrode resistances. The semicircle at high to medium frequency is attributable to the surface layer and interfacial impedance of the electrodes, and the line is due to the Li-ion diffusion within the cathodes.[25-26] From Fig. 3d, it can be seen that MS electrode shows a lower resistance than PMS electrode, indicating a low internal resistance of MS, resulting in better cell performance. This might be due to the larger interlayer distance of MS than that of PMS.

4. CONCLUSIONS

PVP as dispersant was employed successfully to assist the hydrothermal synthesis of MoS_2 to tune the interlayer distance of MoS_2. MoS_2 with larger interlayer distance delivers much more discharge capacity and exhibits more excellent cycling performance comparing with MoS_2 with relative small interlayer distance, indicating the strong interlayer distance dependency of lithium storage of MoS_2. All these are attributed to the internal resistance and Li-ion diffusion in layered MoS_2. Furthermore, PVP could be showed to tune the interlayer distance of MoS_2 by controlling the concentration of PVP, which is underway in our laboratory.

ACKNOWLEDGEMENTS
This work is supported by Education Foundation of Hubei Province (No. T200908), Project of Chinese Ministry of Education (No. 208088).

References

1. V. Etacheri, R. Marom, R. Elazari, G. Salitra and D. Aurbach, *Energ. Environ. Sci.*, 4(2011)3243.
2. B. Scrosati and J. Garche, *J. Power Sources*, 195(2010)2419.
3. M. S. Whittingham, *MRS Bull.*, 33(2008)411.
4. K. Kang, Y. S. Meng, J. Bréger, C. P. Grey and G. Ceder, *Science*, 311(2006)977.
5. J. K. Lee, K. B. Smith, C. M. Hayner and H. H. Kung, *Chem. Commun.*, 46(2010)2025.
6. L.-F. Cui, Y. Yang, C.-M. Hsu and Y. Cui, *Nano Lett.*, 9(2009)3370.
7. M.-H. Park, M. G. Kim, J. Joo, K. Kim, J. Kim, S. Ahn, Y. Cui and J. Cho, *Nano Lett.*, 9(2009)3844.
8. A. Magasinski, P. Dixon, B. Hertzberg, A. Kvit, J. Ayala and G. Yushin, *Nat. Mater.*, 9(2010)353.
9. Y. Li, H. Wang, L. Xie, Y. Liang, G. Hong and H. Dai, *J. Am. Chem. Soc.*, 133(2011)7296.
10. X. Zhou, L.-J. Wan and Y.-G. Guo, *Chem. Commun.*, 49(2013)1838.
11. K. Chang and W. Chen, *Chem. Commun.*, 47(2011)4252.
12. G. Du, Z. Guo, S. Wang, R. Zeng, Z. Chen and H. Liu, *Chem. Commun.*, 46(2010)1106.
13. G. Tang, J. Sun, C. Wei, K. Wu, X. Ji, S. Liu, H. Tang and C. Li, *Mater. Lett.*, 86(2012)9.
14. G. Tang, Y. Wang, W. Chen, H. Tang and C. Li, *Mater. Lett.*, 100(2013)15.
15. H. Li, L. Ma, W.-x. Chen and J.-m. Wang, *Mater. Lett.*, 63(2009)1363.
16. K. Bindumadhavan, S. K. Srivastava and S. Mahanty, *Chem. Commun.*, 49(2013)1823.
17. S. Ding, J. S. Chen and X. W. D. Lou, *Chem. Europ. J.*, 17(2011)13142.
18. C. Zhang, H. B. Wu, Z. Guo and X. W. Lou, *Electrochem. Commun.*, 20(2012)7.
19. H. Li, W. Li, L. Ma, W. Chen and J. Wang, *J. Alloys Compd.*, 471(2009)442.
20. M. Chhowalla and G. A. J. Amaratunga, *Nature*, 407(2000)164.
21. K. Chang and W. Chen, *J. Mater. Chem.*, 21(2011)17175.
22. Y. Miki, D. Nakazato, H. Ikuta, T. Uchida and M. Wakihara, *J. Power Sources*, 54(1995)508.
23. C. Feng, J. Ma, H. Li, R. Zeng, Z. Guo and H. Liu, *Mater. Res. Bull.*, 44(2009)1811.
24. F. Hoshyargar, A. Yella, M. Panthöfer and W. Tremel, *Chem. Mater.*, 23(2011)4716.
25. S. R. Narayanan, D. H. Shen, S. Surampudi, A. I. Attia and G. Halpert, *J. Electrochem. Soc.*, 140(1993)1854.
26. L. Ji, M. Rao, H. Zheng, L. Zhang, Y. Li, W. Duan, J. Guo, E. J. Cairns and Y. Zhang, *J. Am. Chem. Soc.*, 133(2011)18522.